Two-Photon Infrared Resonance Can Enhance Coherent Raman Scattering

Andrew J. Traverso,[1] Brett Hokr,[1] Zhenhuan Yi,[1] Luqi Yuan,[1] Shoichi Yamaguchi,[2]
Marlan O. Scully,[1,3,4] and Vladislav V. Yakovlev[1,*]
[1]*Texas A&M University, College Station, Texas 77843, USA*
[2]*Saitama University, Saitama City 08544, Japan*
[3]*Princeton University, Princeton, New Jersey 08544, USA*
[4]*Baylor University, Waco, Texas 76798, USA*

(Received 31 October 2017; published 6 February 2018)

In this Letter we present a new technique for attaining efficient low-background coherent Raman scattering where the Raman coherence is mediated by a tunable infrared laser in two-photon resonance with a chosen vibrational transition. In addition to the traditional benefits of conventional coherent Raman schemes, this approach offers a number of advantages including potentially higher emission intensity, reduction of nonresonant four-wave mixing background, preferential excitation of the anti-Stokes field, and simplified phase matching conditions. In particular, this is demonstrated in gaseous methane along the ν_1 (A_1) and ν_3 (T_2) vibrational levels using an infrared field tuned between 1400 and 1600 cm^{-1} and a 532-nm pump field. This approach has broad applications, from coherent light generation to spectroscopic remote sensing and chemically specific imaging in microscopy.

DOI: 10.1103/PhysRevLett.120.063602

Introduction.—Raman spectroscopy [1] is a workhorse for probing molecular vibrations. The origin of Raman scattering dates back to the theoretical work of Smekal in 1923 [2], which was soon followed by the landmark experiment of Landsberg and Mandelstam who found the same effect in quartz [3]. By the end of 1928, dozens of papers had already been published on the Raman effect. Physically, Raman scattering involves light with frequency ω_1 scattering inelastically off vibrating molecules such that the scattered (Stokes or anti-Stokes) field has a frequency $\omega_2 = \omega_1 \mp \nu_{bg}$, where ν_{bg} is the molecular vibration frequency. However the (spontaneous) Raman signal is very weak, with only about one pump photon in 10^{10} yielding a useful spontaneous Raman signal photon. But when we consider coherent Raman scattering in which the vibrational levels $|b\rangle$ and $|g\rangle$ of Fig. 1(a) are coherently excited by fields 1 and 2, this increases the signal strength by orders of magnitude. An estimate of coherent enhancement [4–6] is conveyed by the ratio of the number of photons generated through coherent Stokes scattering to the numbers of spontaneously scattered (Stokes) Raman photons, as determined by the coherent density matrix ρ_{bg} in Eq. (1)

$$\frac{\langle n_{4'}^{\mathrm{coh}}\rangle}{\langle n_{4'}^{\mathrm{incoh}}\rangle_{\mathrm{Stokes}}} \cong \lambda_3^2 \frac{N}{V}\frac{|\rho_{bg}|^2}{\rho_{gg}} R, \tag{1}$$

where λ_3 is the probe wavelength, n_4' denotes the generated coherent or incoherent Stokes signal, which is not shown in the figures, N/V is the density, and R is the sample diameter.

Traditional coherent Raman schemes like coherent anti-Stokes Raman scattering (CARS) [Fig. 1(a)] and stimulated Raman scattering (SRS) are already powerful tools [7–11] and continue to be refined [12–14]. These techniques have been implemented in a diverse array of fields for such applications as biomedical imaging, gas and plasma diagnostics, time-resolved spectroscopy, fiber lasers, remote sensing of explosives, and temperature measurements [15–17]. Despite their widespread adoption, there are some inherent drawbacks to these approaches. In particular, sufficiently high intensities are needed to drive these processes. This leads to unwanted effects such as nonresonant background from processes like degenerate four-wave mixing (DFWM) [18] and fluorescence as well as other thermal heating processes that lead to signal distortion or possible burning. Furthermore, given strong enough driving fields in SRS and CARS, competition between the Stokes and anti-Stokes signals can result in signal suppression and limit the overall effective enhancement.

In short, CARS and its derivative FAST CARS are useful techniques. However, it would be interesting to use an IR laser field to generate ρ_{bg} and follow this with $3 \rightarrow 4$ sequentially, as in Fig. 1(c). The good news is that an IR-driven ρ_{bg} would produce a stronger field with fewer lasers. The bad news is that it does not work, since the orientation of the molecules is essential in Raman scattering (see a brief discussion in Supplemental Material [19]), and (sans a surface) this is not present in single-photon IR coherence generation [21]. However, a two-photon IR-driven scheme does work, as in Fig. 1(b).

Here, we demonstrate an approach for coherent Raman generation that not only reduces the nonresonant background, but also achieves excellent signal with modest pump energies. This is accomplished by employing a midinfrared picosecond pump whose frequency is chosen to be in two-photon resonance with a given Raman

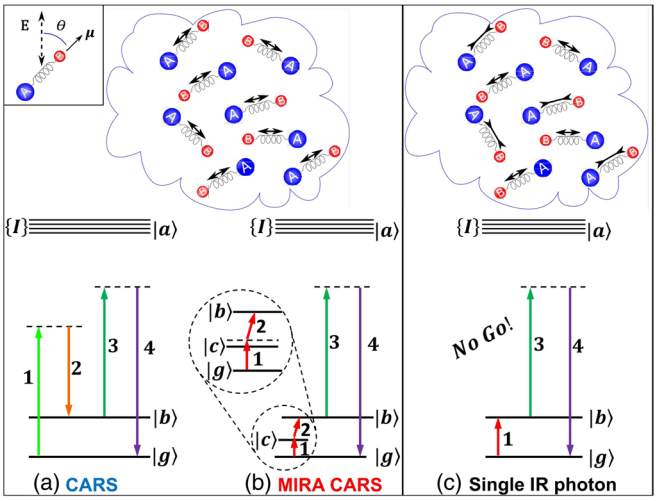

FIG. 1. (a), (b) Two CARS schemes. (a) Typical CARS arrangement where ρ_{bg} coherence is generated by visible lasers 1 and 2. (b) Mid-IR assisted (MIRA) CARS, where ρ_{bg} is generated by mid-IR lasers 1 and 2. The photons at frequencies ω_1 and ω_2 do not need to be equal but could be chosen such that $\omega_1 = \nu_{cg}$ and $\omega_2 = \nu_{bc}$. The two-photon excitation for both CARS and MIRA CARS produce a nonzero ρ_{bg} since all molecules vibrate "in phase." The vibrations are shown schematically as stretching or compressing of the interatomic distance of the molecules. (c) Single photon excitation results in $\rho_{bg} = 0$ when averaged over all molecules since they vibrate "out of phase." Inset: The angle between the electric field $\mathbf{E}$ of the laser and the dipole $\boldsymbol{\mu}$ of the molecule is defined as θ.

transition, as shown in Fig. 1(b). This IR field efficiently couples the ground and excited vibrational state more so than the conventional far-detuned pump and Stokes fields of CARS. Furthermore, we observe a larger enhancement in the anti-Stokes signal relative to the Stokes. Thus with these advantageous characteristics, this approach of MIRA CARS offers a novel platform for spectroscopic detection and imaging with enhanced sensitivity.

MIRA CARS.—To better quantify this mechanism, we start with the MIRA CARS scheme depicted in Fig. 1(b), but will assume that the applied fields $\omega_1 = \omega_2$. Here, the excited state, $|b\rangle$, and the ground state, $|g\rangle$, are two-photon coupled with an IR field generating a coherence, ρ_{bg}, while a third field induces Raman anti-Stokes emission at frequency $\omega_4 = \nu_{bg} + \omega_3$. While MIRA requires $\nu_{bg} = 2\omega_1$ to achieve resonance, the strength of this resonant coherence is strongly dependent on an intermediate allowed transition, $|c\rangle$, that mediates the coupling. This can be understood by examining the derived expression for the coherence,

$$\rho_{bg} \cong \frac{\mu_{bc}E_{\mathrm{IR}}}{\hbar}\frac{\mu_{cg}E_{\mathrm{IR}}}{\hbar}\frac{1}{\gamma}\frac{1}{i(\nu_{cg}-\omega_{\mathrm{IR}})}. \tag{2}$$

Here, γ is the coherence decay for the Raman transition, μ_{mn} is the dipole moment between states $|m\rangle$ and $|n\rangle$, and E_{IR} is the electric field of the two-photon resonant IR laser. For MIRA Raman scattering, the strength of ρ_{bg} is directly proportional to the dipole moments coupling to $|c\rangle$ and inversely proportional to the detuning of the IR pump from $|c\rangle$. These parameters are therefore critically important for determining the efficiency and strength of the generated Raman emission. For comparison, the calculated ρ_{bg} for a conventional CARS scheme transforms the expression as follows:

$$\frac{\mu_{bc}\mu_{cg}}{\gamma}\frac{1}{i(\nu_{cg}-\omega_{\mathrm{IR}})} \Leftrightarrow \frac{\mu_{ba}\mu_{ag}}{\gamma}\frac{1}{i(\nu_{ag}-\omega_{\mathrm{VIS}})}. \tag{3}$$

While it is evident that CARS also requires a dipole-allowed transition to mediate the Raman coherence, this is typically an electronic transition in the visible to ultraviolet regime. Given that the coherence for traditional CARS is prepared using visible or near-infrared fields, this leads to large detunings from the electronic transition. By utilizing a lower energy vibrational transition with a subsequently much smaller detuning, MIRA Raman scattering has the potential to couple far more efficiently.

When estimating these parameters, it is best to consider the general characteristics of molecular transitions. Most molecules possess several low-energy dipole-allowed vibrational transitions with the exact number depending upon the size and composition. Typically, the dipole moments for these vibrational transitions fall in the range of 0.01–1 debye. Moreover, given that the IR photon energies for MIRA are on the order of the vibrational or rotational transitions, the detunings are around 10^2 cm^{-1}. In contrast, the electronic transitions employed in CARS have dipole strengths around 0.1–10 debye with pump detunings on the order of 10^5 cm^{-1}. Thus, MIRA could enhance the generated coherence by a factor of 10–100. With this outlook, MIRA Raman scattering holds promise as a strong spectroscopic technology, which we will demonstrate both through simulation and experiment.

To illustrate the enhanced efficiency and build a framework to compare theory and experiment, we can derive the generalized form of the third-order susceptibility, $\chi^{(3)}$, from the coherence terms in the density matrix approach or through various other methods [22,23]. The $\chi^{(3)}$ coefficients were calculated for the A_1 and T_2 transitions in methane [Fig. 2(a)] for both a CARS scheme as well as our infrared-coupled scheme (see Supplemental Material for details and equations [19]). In particular, a pump and probe wavelength of 800 nm was used for the CARS scheme along with a Stokes field that was scanned across the resonances of the two vibrational transitions. Similarly, a 800-nm probe field was used in the MIRA scheme while the IR field was scanned. In both cases, we used calculated estimates of methane's dipole moments [24], which for the electronic transitions is approximately ~1 debye and ranged from 0.04 to 0.09 debye for the vibrational transitions. The results depicting the relative magnitudes of the total nonlinear susceptibility for each scheme are shown in Fig. 2(c). These are in good qualitative agreement with similar calculations performed previously in different

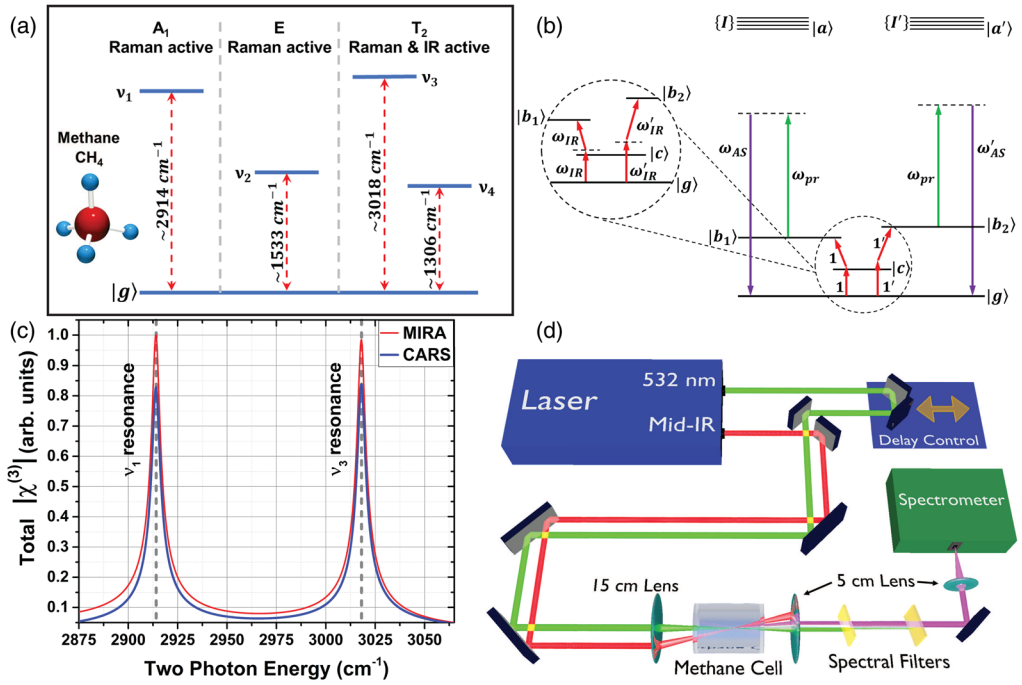

FIG. 2. (a) Vibrational levels of methane. (b) MIRA CARS process for levels $|b_1\rangle \equiv \nu_1$ and $|b_2\rangle \equiv \nu_3$ via $|c\rangle \equiv \nu_4$ in methane. (c) Simulated magnitude of $\chi^{(3)}$ as a function of detuning for an IR-enhanced Raman and traditional CARS schema. MIRA coherent Raman scattering achieves a higher nonlinear susceptibility than traditional CARS. (d) Experimental setup: The IR and 532-nm lasers traveled parallel throughout the beam path with ~1 cm separation, which translated to a 2°–3° angle between them when focused into the cell. The Stokes and anti-Stokes measurements used different spectrometers and spectral filters (see Supplemental Material [19]).

media [25]. Considering the very modest values of the vibrational dipole moments for methane, the $\chi^{(3)}$ coefficient for MIRA still enjoys a substantial increase relative to that of CARS. It is important to note that the actual coherent Raman signal would scale as $|\chi^{(3)}|^2$, which corresponds to a ~40% increase in emission. While promising, this enhancement must hold true for the resonant components of $\chi^{(3)}$ to truly provide an increased Raman signal. The resonant components do in fact achieve a similar level of enhancement as the total $\chi^{(3)}$ such that they closely resemble the trends shown for the total in Fig. 2(c) (see Supplemental Material for resonant component results [19]). Again, this is due to the relative detunings for each scheme where the IR coupling generates coherence more efficiently.

It should be noted that this model only accounts for nonresonant contributions from DFWM at the same frequency as the Raman signal. Other nonresonant processes like fluorescence and DFWM at other frequencies also play a role in lowering the signal-to-noise ratio for traditional CARS schemes. In these cases, MIRA still possesses an inherent advantage due to the lower photon energy of the IR field, which is much less likely to induce fluorescent emission compared to the visible pump fields of CARS. Additionally, the frequency mismatch between the IR field and the visible probe field results in the generated off-resonant frequencies of DFWM to be well detuned from that of the Raman emission. This frequency mismatch also plays into simplifying the phase-matching conditions where the angle to phase match between them is approximately zero [26]. Thus, the Raman emission will essentially be collinear with the probe field, which could be advantageous for some applications such as stand-off spectroscopy.

Experiment.—We chose methane (CH_4) to experimentally demonstrate this technique due to a number of attractive qualities. Methane possesses a fairly simple vibrational structure [Fig. 2(a)] with easily distinguishable spectral lines that are well characterized. Furthermore, it is a ubiquitous molecule, used throughout various industries, and is both biologically and environmentally relevant. Lastly, it is easy to acquire and, being gaseous, provides a good experimental test for potential atmospheric sensing applications. For our interests, we probed the Raman-active transition, ν_1 (A_1), at 2914 cm^{-1}, which corresponds to the C—H bond stretch, as well as the ν_3 (T_2) transition at 3018 cm^{-1}, which is both Raman and dipole allowed.

Figure 2(d) depicts the experimental setup (details can be found in the Supplemental Material [19]). Briefly, two ~30-ps laser pulses, a 532-nm pump pulse, and a tunable mid-IR pulse (2.3 to 10 μm) with maximum energies of 330 and 6 μJ, respectively, were focused into a methane cell, where the two beams crossed at a small angle at the focal point. The generated Stokes and anti-Stokes signals were spectrally filtered and coupled to spectrometers for analysis. Initially, the mid-IR laser was blocked and the spontaneous Raman signal was measured and exhibited a

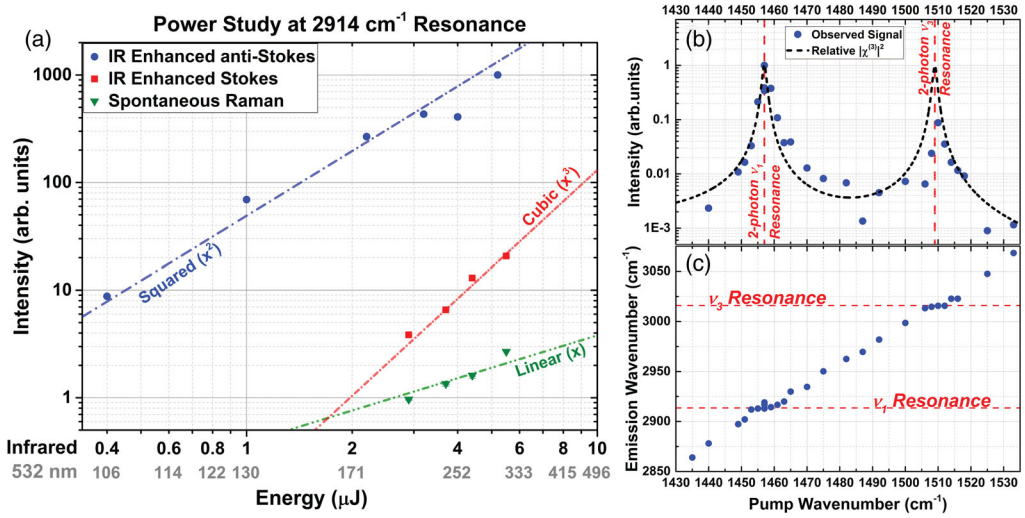

FIG. 3. (a) Power dependence for the MIRA anti-Stokes and Stoke emission as well as the spontaneous Raman Emission. The energies of both the 532-nm pump and IR field at 1457 cm^{-1} were varied simultaneously, as such both energies shown on the x axis. (b) Intensity of observed emission as a function of spectral detuning via the IR laser. The change in Raman intensity qualitatively agrees with the expected values of $|\chi^{(3)}|^2$. (c) Raman wave number versus IR pump wave number. The emission still occurs at the Raman transition wave number when the IR coupled field is slightly detuned from two-photon resonance.

linear dependence as a function of the 532-nm pump energy as plotted in Fig. 3(a).

With the IR laser unblocked, the power dependence of the coherent Raman emission was investigated for both the Stokes and anti-Stokes emissions at the 2914 cm^{-1} ν_1 transition [Fig. 3(a)]. At maximum pump energies the anti-Stokes emission was found to be approximately 50 times more intense than the Stokes emission and over 500 times more intense than the spontaneous Raman signal. Interestingly, given that the energies in both the IR and 532-nm fields were varied simultaneously and three photons are used, one would expect both the Stokes and anti-Stokes emission to follow a cubic trend. This is not the case. As can be seen in Fig. 3(a), while the Stokes does in fact adhere to a cubic trend, the anti-Stokes emission follows the square of the pump energy.

This discrepancy in intensity and power dependence between the anti-Stokes and Stokes fields is indicative that there is a significant asymmetric process occurring during the fields' generation. This decoupling is likely due to slight saturation of the two-photon nonlinear absorption along the vibrational transition. Using the experimental parameters and the definitions outlined in Ref. [27], we estimate the two-photon saturation parameter, $S \gg 1$, and the resonance width, $y \gg 1$, which indicates saturation and homogeneous broadening and are in good agreement with previous studies [27–29]. The observation of this two-photon saturation points to the efficiency with which the coherence is being driven in the MIRA Raman scheme and could potentially be leveraged for other spectroscopic techniques.

Lastly, the frequency of the IR field was swept from 1430 to 1600 cm^{-1}, across the two-photon resonances for both ν_1 and ν_3, while the anti-Stokes emission was monitored. The results of this sweep for both the intensity and wave number of the emission are depicted in Figs. 3(b) and 3(c), respectively. As seen in Fig. 3(b), the observed emission was several orders of magnitude when the IR field was in two-photon resonance with a Raman transition. To further verify, the $\chi^{(3)}$ susceptibility was calculated for a 532-nm pump and the results for $|\chi^{(3)}|^2$ are plotted in Fig. 3(b) along with the experimental data. Here there is fairly good agreement between the observed data and the expected shape of $|\chi^{(3)}|^2$, which should be directly proportional to the emission intensity. The only discrepancy occurs at the ν_3 two-photon resonance where the model overpredicts the expected intensity. This is likely due to the fact that the ν_3 transition is both Raman active and dipole allowed, which means there is a separate loss channel that is not accounted for in the model.

Figure 3(c) demonstrates that when the IR field is detuned far enough from a two-photon resonance, there is no Raman emission. Instead, the measurable emission reverts to a simple nonresonant third-order process of sum frequency mixing between the 532-nm and the IR field ($\omega_{\mathrm{obs}} = \omega_{pr} + 2\omega_{\mathrm{IR}}$), albeit at a much lower intensity. For small nonzero detunings around the two-photon resonances, the observed emission is still centered at the Raman transition frequencies, which further confirms that the induced Raman coherence is the dominant contribution. Moreover, the anti-Stokes emission was also characterized as a function of delay between the mid-IR and 532-nm pulses while the mid-IR pulse was held in two-photon resonance. The anti-Stokes emission was still observed at delay times with no overlap between the pulses, indicating that emission is a product of the generated vibrational coherence and not a nonresonant process like four-wave mixing (see Supplemental Material for more details [19]).

Overall, we have demonstrated efficient coherent coupling with little to no background. This should allow for the detection of Raman signatures with lower pump energies than other schemes. While MIRA Raman scattering offers these advantages, it still delivers the characteristic directional emission and precise spatial and temporal control of traditional CARS. Furthermore, given that the coherent coupling fields are IR fields, this approach could be combined with other complementary spectroscopic techniques, such as Fourier transform infrared spectroscopy, to probe the full vibrational system of a given molecular species with one system. Other implementations could leverage the two-photon saturation to probe certain properties of resonant transitions or control the anti-Stokes or Stokes emission.

Summary and conclusion.—Here, we have demonstrated a new approach utilizing midinfrared fields to significantly enhance coherent Raman scattering. MIRA CARS achieves efficient coherent Raman emission because of the small detunings of the coherence generating IR field as well as the lack of nonresonant contributions like fluorescence and DFWM due to the low IR photon energies. This general approach has the potential for implementation across a wide variety of fields for spectroscopic characterization and imaging. This approach should provide enhanced sensitivity and spectrally selective probing that makes it particularly well suited for molecular gas detection in environmental applications as well as chemical-specific imaging in microscopy.

We acknowledge the support of the National Science Foundation (Division of Biological Infrastructure Awards No. 1455671 and No. 1532188, and Division of Electrical, Communications and Cyber Systems Award No. 1509268), the U.S. Department of Defense (Grant No. FA9550-15-1-0517 and Award No. N00014-16-1-2578) and the Cancer Prevention Research Institute of Texas Grant No. RP160834, Air Force Office of Scientific Research, Office of Naval Research (Award No. N00014-16-1-3054), and the Robert A. Welch Foundation (Grant No. A-1261). This work was also supported by Saitama University Lab-to-Lab Project and Japan Society for the Promotion of Science KAKENHI Grant No. JP15KT0056 and No. JP25104005.

*Corresponding author.
yakovlev@tamu.edu

[1] C. V. Raman and K. S. Krishnan, Nature (London) **121**, 501 (1928).
[2] A. Smekal, Naturwissenschaften **11**, 873 (1923).
[3] G. Landsberg and L. Mandelstam, Naturwissenschaften **16**, 557 (1928).
[4] M. O. Scully, G. W. Kattawar, R. P. Lucht, T. Opatrný, H. Pilloff, A. Rebane, A. V. Sokolov, and M. S. Zubairy, Proc. Natl. Acad. Sci. U.S.A. **99**, 10994 (2002).
[5] G. I. Petrov, R. Arora, V. V. Yakovlev, X. Wang, A. V. Sokolov, and M. O. Scully, Proc. Natl. Acad. Sci. U.S.A. **104**, 7776 (2007).
[6] D. Pestov, G. O. Ariunbold, X. Wang, R. K. Murawski, V. A. Sautenkov, A. V. Sokolov, and M. O. Scully, Opt. Lett. **32**, 1725 (2007).
[7] D. Pestov, X. Wang, G. O. Ariunbold, R. K. Murawski, V. A. Sautenkov, A. Dogariu, A. V. Sokolov, and M. O. Scully, Proc. Natl. Acad. Sci. U.S.A. **105**, 422 (2008).
[8] F. El-Diasty, Vib. Spectrosc. **55**, 1 (2011).
[9] N. Djaker, P.-F. Lenne, D. Marguet, A. Colonna, C. Hadjur, and H. Rigneault, Nucl. Instrum. Methods Phys. Res., Sect. A **571**, 177 (2007).
[10] E. Ploetz, S. Laimgruber, S. Berner, W. Zinth, and P. Gilch, Appl. Phys. B **87**, 389 (2007).
[11] C. W. Freudiger, W. Min, B. G. Saar, S. Lu, G. R. Holtom, C. He, J. C. Tsai, J. X. Kang, and X. S. Xie, Science **322**, 1857 (2008).
[12] C. H. Camp, Jr. and M. T. Cicerone, Nat. Photonics **9**, 295 (2015).
[13] B.-C. Chen and S.-H. Lim, J. Phys. Chem. B **112**, 3653 (2008).
[14] D. Pestov, R. K. Murawski, G. O. Ariunbold, X. Wang, M. Zhi, A. V. Sokolov, V. A. Sautenkov, Y. V. Rostovtsev, A. Dogariu, Y. Huang, and M. O. Scully, Science **316**, 265 (2007).
[15] A. M. Zheltikov, J. Raman Spectrosc. **31**, 653 (2000).
[16] O. Katz, A. Natan, Y. Silberberg, and S. Rosenwaks, Appl. Phys. Lett. **92**, 171116 (2008).
[17] B. H. Hokr, J. N. Bixler, G. D. Noojin, R. J. Thomas, B. A. Rockwell, V. V. Yakovlev, and M. O. Scully, Proc. Natl. Acad. Sci. U.S.A. **111**, 12320 (2014).
[18] M. D. Levenson and S. S. Kano, *Introduction to Nonlinear Laser Spectroscopy (Revised Edition)* (Academic Press, San Diego, CA, 1988).
[19] See Supplemental Material at http://link.aps.org/supplemental/10.1103/PhysRevLett.120.063602 for estimation of single-photon IR-induced coherence and MIRA CARS signal, derived third-order susceptibility for CARS and MIRA CARS and experimental method in detail, which includes Ref. [20].
[20] M. O. Scully and M. S. Zubairy, *Quantum Optics* (Cambridge University Press, Cambridge, England, 1997).
[21] A. V. Sokolov, K. K. Lehmann, M. O. Scully, and D. Herschbach, Phys. Rev. A **79**, 053805 (2009).
[22] R. W. Boyd, *Nonlinear Optics*, 3rd ed. (Academic Press, Burlington, MA, 2008), p. 613.
[23] J. F. Reintjes, *Nonlinear Optical Parametric Processes in Liquids and Gases* (Academic Press, Cambridge, MA, 1984), pp. 1–466.
[24] S. N. Yurchenko, J. Tennyson, R. J. Barber, and W. Thiel, J. Mol. Spectrosc. **291**, 69 (2013).
[25] R. B. Miles and S. E. Harris, IEEE J. Quantum Electron. **9**, 470 (1973).
[26] S. Chandra, A. Compaan, and E. Wiener-Avnear, J. Raman Spectrosc. **10**, 103 (1981).
[27] J. F. Ward and A. V. Smith, Phys. Rev. Lett. **35**, 653 (1975).
[28] A. T. Georges, P. Lambropoulos, and J. H. Marburger, Opt. Commun. **18**, 509 (1976).
[29] C. C. Wang and L. I. Davis, Jr., Phys. Rev. Lett. **35**, 650 (1975).